Research Article | Vol. 26, No. 5 | 5 Mar 2018 | OPTICS EXPRESS 5292
Optics EXPRESS

Refractive-index-modified-dot Fabry-Perot fiber probe fabricated by femtosecond laser for high-temperature sensing

PENGCHENG CHEN AND XUEWEN SHU*

Wuhan National Laboratory for Optoelectronics & School of Optical and Electronic Information, Huazhong University of Science and Technology, Wuhan 430074, China
xshu@hust.edu.cn

Abstract: An optical fiber Fabry-Perot probe sensor for high-temperature measurement is proposed and demonstrated, which is fabricated by inducing a refractive-index-modified-dot (RIMD) in the fiber core near the end of a standard single mode fiber (SMF) using a femtosecond laser. The RIMD and the SMF end faces form a Fabry-Perot interferometer (FPI) with a high-quality interference fringe visibility (>20dB). As a high-temperature sensor, such an FPI exhibits a sensitivity of 13.9 pm/°C and 18.6 pm/°C in the range of 100-500 °C and 500-1000 °C, respectively. The fabrication process of this device is quite straightforward, simple, time saving, and the sensor features small size, ease of fabrication, low cost, assembly-free, good mechanical strength, and high linear sensitivity.

OCIS codes: (050.2230) Fabry-Perot; (060.2310) Fiber optics; (060.2340) Fiber optics components; (060.2370) Fiber optics sensors; (140.3390) Laser materials processing.

References and links

1. V. de Oliveira, M. Muller, and H. J. Kalinowski, "Bragg gratings in standard nonhydrogenated fibers for high-temperature sensing," Appl. Opt. **50**(25), E55–E58 (2011).
2. G. Rego, O. Okhotnikov, E. Dianov, and V. Sulimov, "High-temperature stability of long-period fiber gratings produced using an electric arc," J. Lightwave Technol. **19**(10), 1574–1579 (2001).
3. A. A. Jasim, S. W. Harun, H. Arof, and H. Ahmad, "Inline Microfiber Mach-Zehnder Interferometer for High Temperature Sensing," IEEE Sens. J. **13**(2), 626–628 (2013).
4. J. E. Antonio-Lopez Z. S. Eznaveh, P. L. Wa, A. Schulzgen, and R. Amezcua-Correa, "Multicore fiber sensor for high-temperature applications up to 1000 degrees C," Opt. Lett. **39**(15), 4309–4312 (2014).
5. A. Van Newkirk, E. Antonio-Lopez, G. Salceda-Delgado, R. Amezcua-Correa, and A. Schülzgen, "Optimization of multicore fiber for high-temperature sensing," Opt. Lett. **39**(16), 4812–4815 (2014).
6. X. Hu, X. Shen, J. Wu, J. Peng, L. Yang, J. Li, H. Li, and N. Dai, "All fiber M-Z interferometer for high temperature sensing based on a hetero-structured cladding solid-core photonic bandgap fiber," Opt. Express **24**(19), 21693–21699 (2016).
7. J. J. Zhu, A. P. Zhang, T. H. Xia, S. L. He, and W. Xue, "Fiber-Optic High-Temperature Sensor Based on Thin-Core Fiber Modal Interferometer," IEEE Sens. J. **10**(9), 1415–1418 (2010).
8. B. Dong, L. Wei, and D. P. Zhou, "Miniature high-sensitivity high-temperature fiber sensor with a dispersion compensation fiber-based interferometer," Appl. Opt. **48**(33), 6466–6469 (2009).
9. X. L. Tan, Y. F. Geng, X. J. Li, Y. Q. Yu, Y. L. Deng, Z. Yin, and R. Gao, "Core Mode-Cladding Supermode Modal Interferometer and High-Temperature Sensing Application Based on All-Solid Photonic Bandgap Fiber," IEEE Photonics J. **6**(1), 1–7 (2014).
10. J. Yang, Y. Zheng, L. H. Chen, C. C. Chan, X. Dong, P. P. Shum, and H. Su, "Miniature temperature sensor with germania-core optical fiber," Opt. Express **23**(14), 17687–17692 (2015).
11. N. Zhao, H. Fu, M. Shao, X. Yan, H. Li, Q. Liu, H. Gao, Y. Liu, and X. Qiao, "High temperature probe sensor with high sensitivity based on Michelson interferometer," Opt. Commun. **343**, 131–134 (2015).
12. L. Duan, P. Zhang, M. Tang, R. Wang, Z. Zhao, S. Fu, L. Gan, B. Zhu, W. Tong, D. Liu, and P. P. Shum, "Heterogeneous all-solid multicore fiber based multipath Michelson interferometer for high temperature sensing," Opt. Express **24**(18), 20210–20218 (2016).
13. L. V. Nguyen, D. Hwang, S. Moon, D. S. Moon, and Y. Chung, "High temperature fiber sensor with high sensitivity based on core diameter mismatch," Opt. Express **16**(15), 11369–11375 (2008).
14. Y. Y. Yu, L. Jiang, B. Y. Li, S. M. Wang, and H. B. Wu, "High-temperature reflective sensor based on single fusion-splicing fiber taper without coating," Chin. Opt. Lett. **10**(12), 122801 (2012).
15. L. Xu, L. Jiang, S. Wang, B. Li, and Y. Lu, "High-temperature sensor based on an abrupt-taper Michelson interferometer in single-mode fiber," Appl. Opt. **52**(10), 2038–2041 (2013).

#318843 https://doi.org/10.1364/OE.26.005309
Journal © 2018 Received 3 Jan 2018; revised 8 Feb 2018; accepted 11 Feb 2018; published 21 Feb 2018

Optics EXPRESS

16. C.-L. Lee, J.-M. Hsu, J.-S. Horng, W.-Y. Sung, and C.-M. Li, "Microcavity Fiber Fabry-Perot Interferometer With an Embedded Golden Thin Film," IEEE Photonics Technol. Lett. **25**(9), 833–836 (2013).
17. Y. Zhu, Z. Huang, F. Shen, and A. Wang, "Sapphire-fiber-based white-light interferometric sensor for high-temperature measurements," Opt. Lett. **30**(7), 711–713 (2005).
18. H. Y. Choi, K. S. Park, S. J. Park, U.-C. Paek, B. H. Lee, and E. S. Choi, "Miniature fiber-optic high temperature sensor based on a hybrid structured Fabry-Perot interferometer," Opt. Lett. **33**(21), 2455–2457 (2008).
19. J. Villatoro, V. Finazzi, G. Coviello, and V. Pruneri, "Photonic-crystal-fiber-enabled micro-Fabry-Perot interferometer," Opt. Lett. **34**(16), 2441–2443 (2009).
20. H. Y. Choi, G. Mudhana, K. S. Park, U. C. Paek, and B. H. Lee, "Cross-talk free and ultra-compact fiber optic sensor for simultaneous measurement of temperature and refractive index," Opt. Express **18**(1), 141–149 (2010).
21. M. S. Ferreira, L. Coelho, K. Schuster, J. Kobelke, J. L. Santos, and O. Frazão, "Fabry-Perot cavity based on a diaphragm-free hollow-core silica tube," Opt. Lett. **36**(20), 4029–4031 (2011).
22. C. Wu, H. Y. Fu, K. K. Qureshi, B. O. Guan, and H. Y. Tam, "High-pressure and high-temperature characteristics of a Fabry-Perot interferometer based on photonic crystal fiber," Opt. Lett. **36**(3), 412–414 (2011).
23. F. C. Favero, R. Spittel, F. Just, J. Kobelke, M. Rothhardt, and H. Bartelt, "A miniature temperature high germanium doped PCF interferometer sensor," Opt. Express **21**(25), 30266–30274 (2013).
24. M. S. Ferreira, P. Roriz, J. Bierlich, J. Kobelke, K. Wondraczek, C. Aichele, K. Schuster, J. L. Santos, and O. Frazão, "Fabry-Perot cavity based on silica tube for strain sensing at high temperatures," Opt. Express **23**(12), 16063–16070 (2015).
25. J. Zhang, H. Sun, Q. Rong, Y. Ma, L. Liang, Q. Xu, P. Zhao, Z. Feng, M. Hu, and X. Qiao, "High-temperature sensor using a Fabry-Perot interferometer based on solid-core photonic crystal fiber," Chin. Opt. Lett. **10**(7), 070607 (2012).
26. Y. Du, X. Qiao, Q. Rong, H. Yang, D. Feng, R. Wang, M. Hu, and Z. Feng, "A Miniature Fabry-Perot Interferometer for High Temperature Measurement Using a Double-Core Photonic Crystal Fiber," IEEE Sens. J. **14**(4), 1069–1073 (2014).
27. X. Tan, Y. Geng, X. Li, R. Gao, and Z. Yin, "High temperature microstructured fiber sensor based on a partial-reflection-enabled intrinsic Fabry-Perot interferometer," Appl. Opt. **52**(34), 8195–8198 (2013).
28. D. W. Duan, Y. J. Rao, Y. S. Hou, and T. Zhu, "Microbubble based fiber-optic Fabry-Perot interferometer formed by fusion splicing single-mode fibers for strain measurement," Appl. Opt. **51**(8), 1033–1036 (2012).
29. J. Mathew, O. Schneller, D. Polyzos, D. Havermann, R. M. Carter, W. N. MacPherson, D. P. Hand, and R. R. J. Maier, "In-Fiber Fabry-Perot Cavity Sensor for High-Temperature Applications," J. Lightwave Technol. **33**(12), 2419–2425 (2015).
30. Z. Liu, X. Qiao, and R. Wang, "Miniaturized fiber-taper-based Fabry-Perot interferometer for high-temperature sensing," Appl. Opt. **56**(2), 256–259 (2017).
31. J. L. Kou, J. Feng, L. Ye, F. Xu, and Y. Q. Lu, "Miniaturized fiber taper reflective interferometer for high temperature measurement," Opt. Express **18**(13), 14245–14250 (2010).
32. R. M. André, S. Pevec, M. Becker, J. Dellith, M. Rothhardt, M. B. Marques, D. Donlagic, H. Bartelt, and O. Frazão, "Focused ion beam post-processing of optical fiber Fabry-Perot cavities for sensing applications," Opt. Express **22**(11), 13102–13108 (2014).
33. T. Wei, Y. Han, H. L. Tsai, and H. Xiao, "Miniaturized fiber inline Fabry-Perot interferometer fabricated with a femtosecond laser," Opt. Lett. **33**(6), 536–538 (2008).
34. Y. Liu, S. Qu, and Y. Li, "Single microchannel high-temperature fiber sensor by femtosecond laser-induced water breakdown," Opt. Lett. **38**(3), 335–337 (2013).
35. P. Chen, X. Shu, H. Cao, and K. Sugden, "Ultra-sensitive refractive index sensor based on an extremely simple femtosecond-laser-induced structure," Opt. Lett. **42**(6), 1157–1160 (2017).

1. Introduction

Over the past few decades, optical fiber sensors for harsh conditions in various industries, such as high-temperature in oil exploration, high-power electrical systems, and tunnel fire alarms, have attracted growing interest due to their many intrinsic advantages such as compact size, light weight, immunity to electromagnetic interference, electrically passive operation and long life.

Various fiber high-temperature sensors have been developed, including fiber Bragg gratings (FBGs), long-period fiber gratings (LPFGs), and fiber interferometers such as Mach-Zehnder interferometers (MZIs), Michelson interferometers (MIs) and Fabry-Perot interferometers (FPIs). Among them, FBG-based high-temperature sensors are widely used, but standard gratings suffer from erasure at temperature above 800 °C [1] and require to control strict periodicity, limiting their applications. LPFG-based high-temperature sensors [2] have a large cross sensitivity to fiber bending or strain, and they are relatively long (usually several centimeters). Various schemes including fiber tapers [3], special fibers fusion

Optics EXPRESS

splicing [4–12] and mismatched core diameter structures [11,13–15] have been exploited to construct MZIs and MIs. However, MZIs work in transmission, which are not very compact, not suitable for working in narrow space and remote sensing. MIs are reflective probes, but their size are still not small enough. Besides, structures with fiber tapers, fusion splicing and mismatched cores usually have very poor mechanical strength. Compared with MZIs and MIs, FPIs are far more compact, simple and suitable for working in narrow space and remote sensing.

FPI high-temperature sensors are also fabricated by various techniques, including diaphragm-based [16,17], special fiber-based [18–27], multi-fusion splicing-based [28,29], chemical etching-based [30], FIB-based [31,32] and laser micromachining-based [33,34]. The sensors created with the first four techniques are assembly ones, which usually need to assemble multiple separated components together with a fusion splicer. Thus, the length of the cavity is difficult or impossible to be precisely controlled. Moreover, special fiber is high cost; diaphragm or multi-fusion splicing involves complex manufacturing steps; chemical etching is dangerous. The fabrication process of FIB-based FPI is time-consuming, complicated and high cost. The reported sensors based on laser micromachining technique are mainly based on laser ablation effect, such as directly cutting a groove on SMF to form FPI [33] or drilling a microchannel through fiber core [34] with a femtosecond laser (fs-laser). However, the groove cavity FPI has poor mechanical strength as the most part of the fiber has been removed. Besides, the layer-by-layer fabrication process is time-consuming and complex. The mechanical strength of the micro-channel FPI is still not good enough because part of the cladding is removed. Moreover, an extra arc discharge procedure is required to smooth the microchannel sidewalls to obtain a high fringe contrast.

In this paper, we propose and demonstrate a new high temperature sensor based on an assembly-free robust FPI formed with a refractive-index-modified-dot (RIMD) near the end of a SMF. Previously, we have used such a FPI for refractive index sensing [35], however it had a very low fringe visibility in the air (only ~0.8dB) and thus is not suitable for high temperature measurement. Here we show that by properly adjust the fabrication condition (such as increasing the fs-laser pulse energy), high-fringe-visibility (>20dB) FPIs can also be achieved, which are suitable for wavelength demodulation based high temperature sensing. Compared with the previously published fiber sensors based on fs-laser ablation effect [33, 34], the proposed RIMD based FPI sensor is much simpler, more robust, more efficient in fabrication and more cost saving. Experiment results confirmed that such a structure is very suitable for high-temperature measurement and exhibits a good linear sensitivity of 13.9 and 18.6 pm/°C in the range of 100-500 °C and 500-1000 °C , respectively.

2. Experimental setup and fabrication of the FPI

The schematic structure of our proposed FPI is illustrated in Fig. 1(a). The device was fabricated by a fs-laser system (Spectra-Physics) with a center wavelength, repetition rate and pulse duration of 520nm, 200kHz, 350fs, respectively. A broadband source (BBS), a fiber circulator and an optical spectrum analyzer (OSA, YOKOGAWA, AQ6370C) were connected to real-time monitor the reflection spectrum during the fabrication. The fabrication of the FPI is quite straight-forward. First, an end well cleaved SMF (YOFC, G.652) was mounted on a 3-D translation stage (Newport). Then, the stage is adjusted to position the SMF correctly. Last, the fiber is exposed to fs-laser pulses to generate a refractive-index-modified-dot (RIMD). An online monitoring CCD system was used to monitor the sample morphology during the direct writing process. In the fabrication, the laser was focused through a microscope objective (Olympus UMPLFL 40X) with a numerical aperture (NA) of 0.65 and the actual fs-laser energy used for fabrication was approximately 4μJ/pulse, which is much stronger than that used in [35]. Figures 1(b) and 1(c) show the top and the side view of microscope images of a fabricated FPI, respectively.

Optics EXPRESS

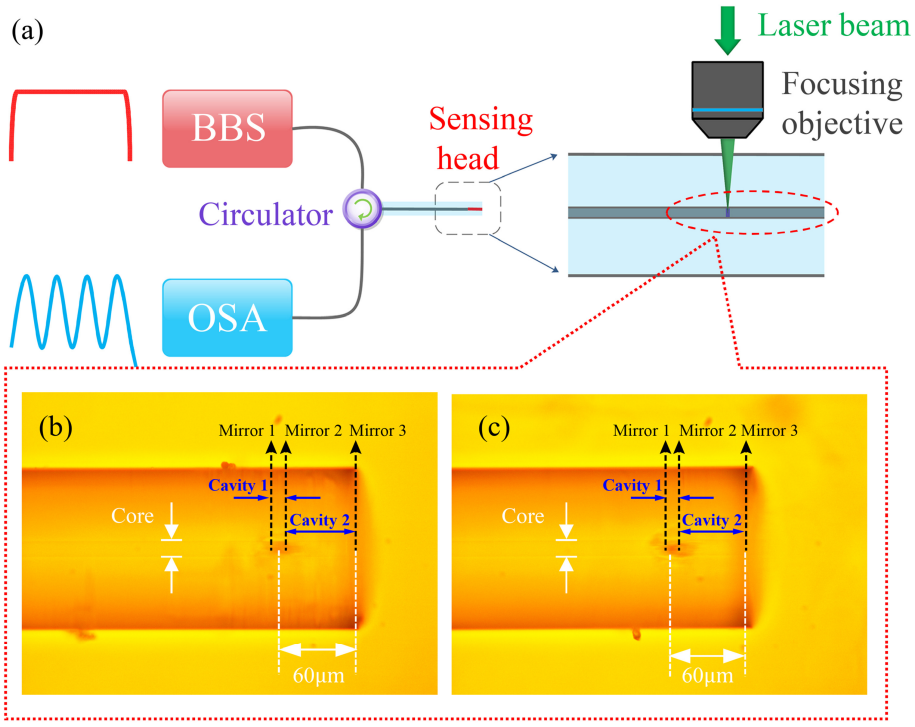

Fig. 1. (**a**) System schematic for inducing a refractive index modified dot in fiber core using a femtosecond laser to form FPI. (**b**) The top and the side (**c**) view of microscope images of the fabricated FPI.

3. Operation principle

For the proposed FPI, the normalized reflection intensity can be modeled with three-beam optical interference equation [35]:

$$I = R_1 + A^2 R_2 + B^2 R_3 - 2\sqrt{R_1 R_2}\, A\cos(2\varphi_1) - 2\sqrt{R_1 R_3}\, B\cos(2\varphi_1 + 2\varphi_2) + 2AB\sqrt{R_2 R_3}\cos(2\varphi_2) \quad (1)$$

where

I is the normalized reflection intensity;

R_i is the reflection of the three Mirrors, i ($i = 1, 2, 3$);

$R_1 = R_2 = [\Delta n / (n_{dot} + n_{co})]^2$, $R_3 = [(n_{co} - 1) / (n_{co} + n_{dot})]^2$; n_{co} is the core RI of SMF, n_{dot} is the RI of the RIMD and Δn is the RI change induced by fs-laser.

$A = (1-\alpha_1)(1-\gamma_1)(1-R_1)$;

$B = (1-\alpha_1)(1-\gamma_1)(1-R_1)(1-\alpha_2)(1-\gamma_2)(1-R_2)$;

α_1, α_2 are the intensity attenuation factors of the Mirror 1 and Mirror 2, respectively;

γ_1, γ_2 are the transmission loss factors of the cavity 1 and cavity 2, respectively;

$\varphi_j = 4\pi n_j L_j / \lambda$ is the phase shift in the cavity j ($j = 1, 2$);

n_j is the effective RI of the cavity j;

L_j is the length of the cavity j;

λ is the free space wavelength.

Optics EXPRESS

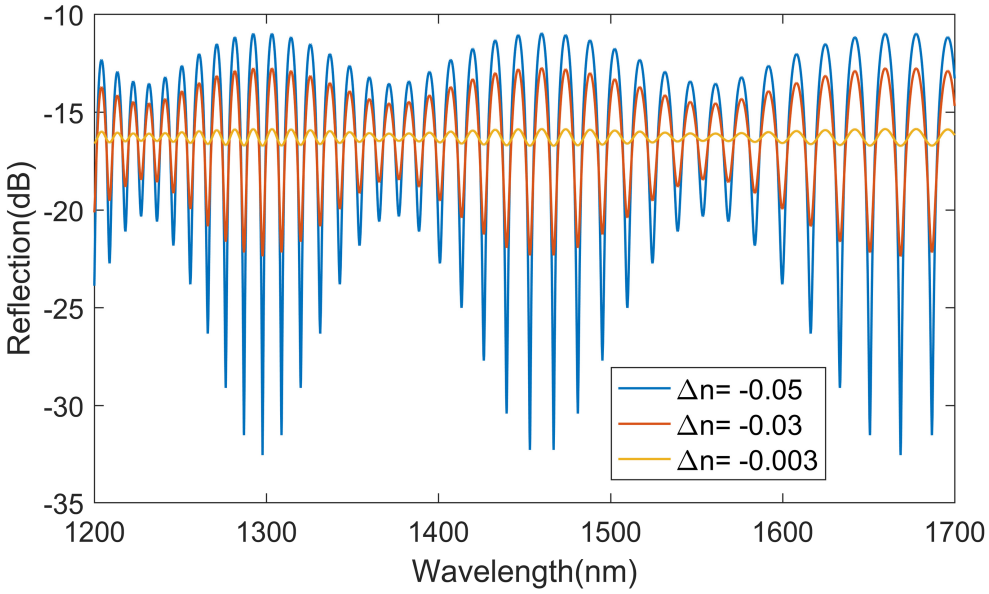

Fig. 2. Calculated reflection spectra for different Δn .

Using Eq. (1), we calculate the normalized reflection spectra of such a structure with different Δn . Other parameters used in the simulation are $\alpha_1 = \alpha_2 = 0.56$, $\gamma_1 = \gamma_2 = 0.11$, $n_{co} = 1.46$, $L_1 = 4\mu m$, $L_2 = 50\mu m$. Figure 2 shows the calculated spectra for the $\Delta n = -0.05$, -0.03 and -0.003, respectively. Obviously, the fringe contrast increases when the Δn changing from -0.003 to -0.05, which means that a high-fringe-contrast FPI can be obtained by adjusting the femtosecond laser fabrication condition to introduce strong refractive index change.

The dense free spectral range (FSR) corresponding to the long cavity can be derived as:

$$FSR \approx \frac{\lambda^2}{2n_{co}L_2} \tag{2}$$

The temperature sensitivity of the dense fringes of the FPI probe can be obtained by:

$$S = \frac{\partial \lambda}{\partial T} = \left(\frac{1}{n_{co}} \frac{\partial n_{co}}{\partial T} + \frac{1}{L_2} \frac{\partial L_2}{\partial T} \right) \lambda = (\alpha_T + \xi_T)\lambda \tag{3}$$

where α_T is the thermo-optic coefficient and ξ_T is the thermal expansion coefficient. It is obvious that by monitoring the wavelength shift of the reflection spectrum, the temperature can be measured in real time.

Optics EXPRESS

4. Result and discussion

4.1 Spectra of the FPI with different cavity length

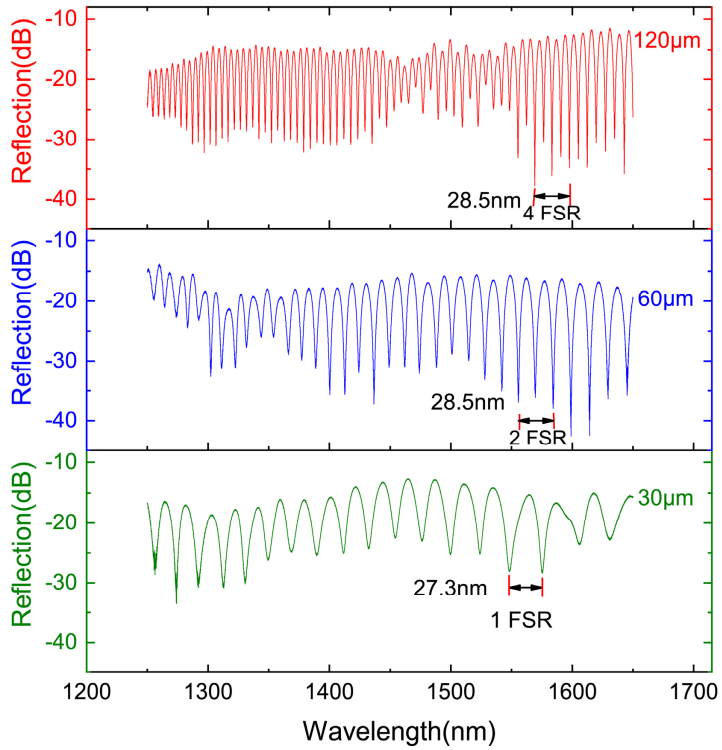

Fig. 3. Measured reflection spectra of FPI probes with different cavity lengths (**a**) 120μm, (**b**) 60μm and (**c**) 30μm.

By changing the distance between the RIMD and the SMF end face, FPI probes with different cavity length can be easily achieved. Figure 3 shows the measured reflection spectra of three FPIs samples with a cavity length of 120, 60 and 30 μm, respectively. The maximum fringe contrast of the FPIs is more than 20dB. Clearly, when the cavity length is halved, the FSR is doubled. It means that FSR is inversely proportional to the cavity length, which is in good consistency with the theoretical calculation explained by Eq. (2). One may also note that the secondary periods of these samples are much less clear (compared with the simulation) and appear to be some different, which indicate that the RIMDs formed in these samples are not perfect spheres and also slightly different in sizes. This can be improved if one carefully controls the beam shape and focus spots of the fs-laser.

4.2 High-temperature response and discussion

Before investigating the response of the probe to high-temperature, we first put the device in a tube furnace, being heating at 1000 °C and maintained for 10h to eliminate residual stress in the fiber. Then, it was naturally cooled down to room temperature. After the annealing process, the sensor probe was tested stepwise by heating up and cooling down with a temperature step of 50 °C , respectively. Figure 4 shows the measured spectral response of the FPI sensor with 60μm cavity length, where the fringe dips at each temperature step during the heating process are compared, and an obvious monotonic red shift with the increase of temperature is noted.

Optics EXPRESS

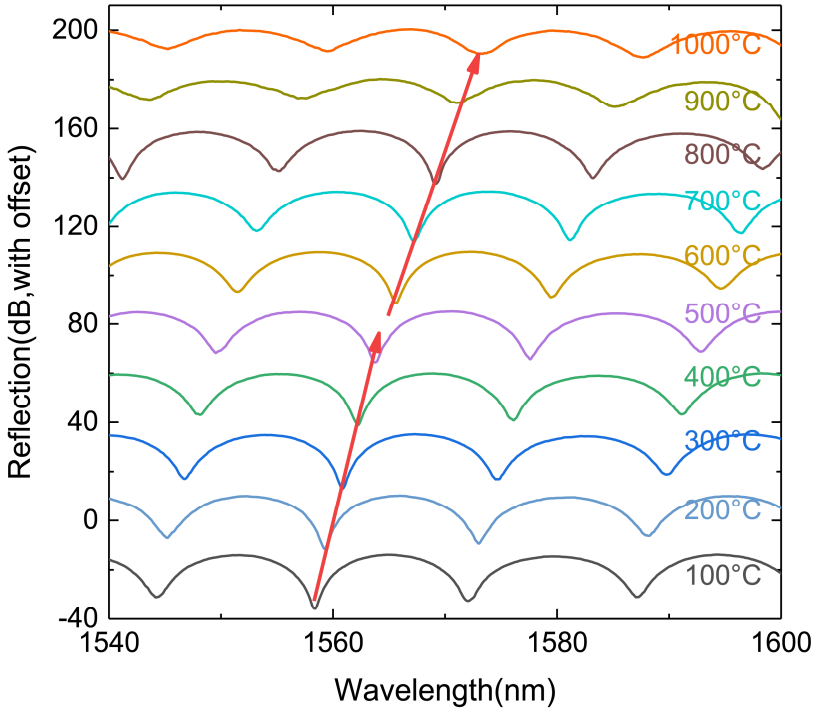

Fig. 4. Spectral response of a FPI probe with 60 μm cavity length at different temperatures.

The interference dip at initial wavelength ~1558nm was chosen to monitor its wavelength shift versus temperature, as shown in Fig. 4. Figure 5 shows the measured wavelength shift the selected interference dip during the heating and cooling cycle. Two-order polynomial function:

$$\lambda = \mathrm{B}_2 T^2 + \mathrm{B}_2 T + \mathrm{Intercept}$$

is used to fit the experimental results. The corresponding function coefficients of heating and cooling are shown in Fig. 5, and the correlation coefficient (R^2) are 0.99936 and 0.99962, respectively.

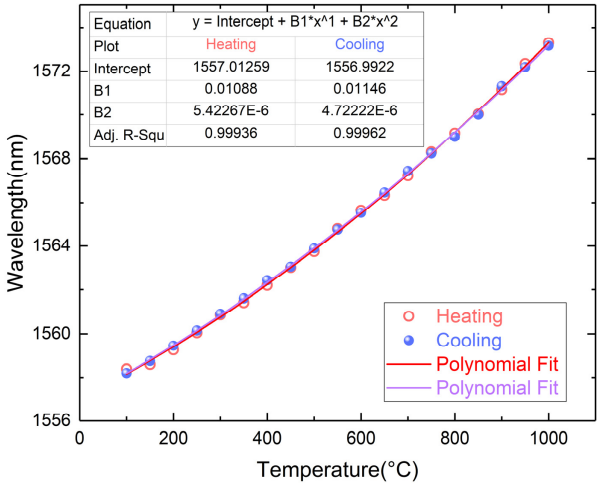

Fig. 5. Interference dip wavelength at ~1558nm with temperature variation for the heating and cooling cycle.

Optics EXPRESS

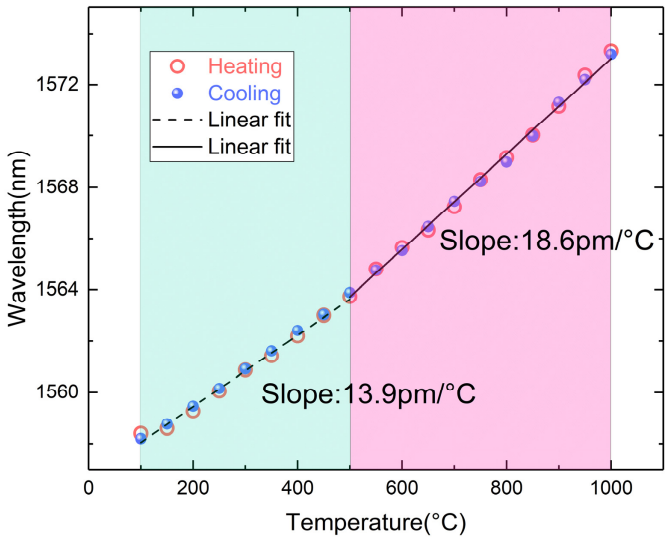

Fig. 6. Linear fit at low temperature and high temperature.

We find that the temperature region can be also divided into two parts with good linear fitting, as shown in Fig. 6. For the lower temperature range of 100-500 °C , a linear sensitivity of ~13.9 pm/°C is obtained (R^2 = 0.99414 and 0.99865 for the heating and cooling cycle, respectively). For the higher temperature range of 500-1000 °C , a linear sensitivity of ~18.6 pm/°C is obtained (R^2 = 0.99713 and 0.99681 for the heating and cooling cycle, respectively). The thermal expansion coefficient of silica is $0.55 \times 10^{-6}\ °C^{-1}$, the thermo-optic coefficient of silica is $8.3 \times 10^{-6}\ °C^{-1}$ [22]. According to Eq. (3), the temperature sensitivity is calculated to be 13.8 pm/°C, which is very close to experimental sensitivity (13.9 pm/°C). The wavelength sensitivity to high temperature of the SMF-based FPIs is typically in the range of 12- 18 pm/°C [16, 22, 25–27, 30, 34]. Obviously, our FPI is in good agreement with the theoretical calculation and the previously reported results. The resolution could be estimated to be ~0.7 °C considering that the resolution of the OSA is 0.01 nm.

5. Conclusion

In summary, we proposed and demonstrated a new high temperature sensor based on a high-fringe-visibility (>20dB) FPI formed by inducing a strong refractive-index-modified-dot (RIMD) in a SMF core using fs-laser. Such a FPI is very suitable for high-temperature measurement and exhibits a sensitivity of 13.9 pm/°C and 18.6 pm/°C in the range of 100-500 °C and 500-1000 °C, respectively. The excellent features of a simple structure, ease of fabrication, ultra-compact, low-cost, assembly-free and high-linearity sensitivity could make it promising in the practical harsh conditions in various industrial fields.

Funding

National Natural Science Foundation of China (NSFC) (61775074); National 1000 Young Talents Program, China; 111 Project (No. B07038)